IEEE Access
Multidisciplinary ⋮ Rapid Review ⋮ Open Access Journal

Received 3 August 2023, accepted 23 August 2023, date of publication 4 September 2023, date of current version 11 September 2023.

Digital Object Identifier 10.1109/ACCESS.2023.3311755

RESEARCH ARTICLE

A Communication-Free and Model-Free Predictive Control for a Dynamic IPT System With High Power Factor for Electric Vehicles

SINA NAVAIYAN KALAT[1], SADEGH VAEZ-ZADEH[1,2], (Senior Member, IEEE), ALI ZAKERIAN[1], AMIR BABAKI[3], (Member, IEEE), AND THOMAS EBEL[3], (Senior Member, IEEE)

[1]Advanced Motion Systems Research Laboratory, School of Electrical and Computer Engineering, College of Engineering, University of Tehran, Tehran 14395-515, Iran
[2]Center of Excellence on Applied Electromagnetic Systems, School of Electrical and Computer Engineering, College of Engineering, University of Tehran, Tehran 14395-515, Iran
[3]Center for Industrial Electronics (CIE), Department of Mechanical and Electrical Engineering, University of Southern Denmark, 6400 Sønderborg, Denmark

Corresponding author: Sadegh Vaez-Zadeh (vaezs@ut.ac.ir)

This work was supported in part by the IE-Industrial Elektronik Project, which has received EU Co-Financing from the European Social Fund under Grant SFD-17-0036; and in part by the Iran National Science Foundation (INSF) through the Chair of Contactless and Wireless Power Transfer under Project 940013.

ABSTRACT Facilitating charging of Electric Vehicles (EVs), dynamic Inductive Power Transfer (IPT) technology has recently gained considerable attention. Yet, stabilizing the transferred power under different load resistances and coupling coefficients is still an issue. On the other hand, realizing high power factor (PF) operation in constant voltage (CV) operation increases the life of equipment in the system. A new model-free predictive control (MFPC) for DWPT systems is proposed in this paper based on the frequency optimization. The imaginary part of the input impedance is expressed as a function mega parameter. The control system becomes independent of the system parameter by calculating the mega parameters. Also, the group-based control approach used in the MFPC method, reduces the computing burden, improves the system dynamics, and avoids unsafe operating points. Moreover, the system output voltage is regulated by adjusting the duty cycle of the inverter. Simulation and experimental results validate the effectiveness of the proposed method.

INDEX TERMS Constant voltage, dynamic inductive power transfer, electric vehicles, frequency optimization, group-based control, model-free predictive control, power factor.

I. INTRODUCTION

Inductive power transfer (IPT) is gaining considerable attention due to its benefits, including convenience, safety, and flexibility. In dynamic inductive power transfer systems used for charging moving electric vehicles (EVs), the demanded power is dynamically met via the coils placed beneath the road's surface [1]. The two sides of such an IPT system can operate independently [2]. However, the system should be able to maintain a reliable transferred power with a minimum VA rating of the power supply against variable load resistance and coils coupling coefficient. Therefore, reducing the reactive power flowing through the high-frequency inverter is indispensable to avoid system overdesign.

The primary and secondary sides' resonant frequencies are often considered equal in the literature [3]. In this case, applying the resonant frequency leads to the unity power factor (PF) operation, maximizes the apparent input power per ampere, and reduces the inverter switching loss [4]. However, there is no warranty that the resonant frequencies would be equal in practice. For instance, the secondary side compensator capacitor may deviate from its designed value. Hence, the secondary side resonant frequency may be different from the ones on the primary side. Moreover, the circuit

The associate editor coordinating the review of this manuscript and approving it for publication was Wonhee Kim.

components' aging may also change both sides' resonant frequencies. Thus, the unity *PF* operation no longer occurs for operation at the system resonant frequency [5]. Using a single stage power factor correction has been studied In [6] to overcome the efficiency issue in two stage topologies but it can increase the complexity of control. In [7] a complete optimum design procedure of inductor in two stage PFC and WPT system have been investigated, however, it suffers a drop of overall efficiency in the system. The optimum operating frequency depends on the coupling coefficient, k, and load resistance of the IPT system. As those parameters vary by EVs movement on the charging lane, it is essential to determine them dynamically.

Tracking methods have been proposed in the literature to maximize *PF*, using a coupling coefficient estimator and an extra buck-boost converter on the secondary side [8], [9]. Frequency tracking has also been proposed to maximize the system *PF* to reduce the reactive input power [10]. However, applying different frequencies to the system without knowing the system response may lead to unsafe operating points.

To improve the dynamic performance of IPT systems, researchers have proposed various control strategies. An optimized PID control design method has been proposed in [11]. Although the overall dynamic performance of the system is enhanced, the system still suffers from the inherent sluggishness of the PID controller. Sliding mode control can achieve better dynamic performances in response to circuit parameter changes [12]. However, the complex modeling process makes the controller design complicated. On the other hand, each designed controller is based on a unique operating point. Thus, a new operating point needs a new controller design. In other words, the independency of the designed controller from the model has yet to be addressed as a problem.

Model-based Predictive Control (MPC) is a promising control strategy that uses a mathematical model-based algorithm to predict the system state and selects the optimum control sequence [13], [14]. It minimizes a specified cost function over a particular prediction horizon. Meanwhile, the precise system model cannot be achieved in practice. Accurate values of system parameters may not be available to the controller. On the other hand, even if the values are available, they may vary due to different driving conditions, aging effects, and misalignment of EV [15]. Therefore, reducing the control system dependency on system models and parameters is of interest.

The moving discretized control set model predictive control (MDCS-MPC) represents the state-of-the-art of model predictive control in power converters [16]. It is aimed to reduce the number of calculations needed in each switching period. It also leads to a lower computational burden. The method has been applied to the dual-active bridge converter and can be easily applied to IPT systems as well [17]. In this method, the controller gradually searches for the optimum control variable by evaluating a small subset of the discretized control set (DCS) during each control interval. Hence, it is more suitable for fine-level control when the system output is close to the steady-state value. Under significant disturbances, however, MDCS may suffer from a slow dynamic response, especially when the resolution of the DCS is high.

In [18], a load estimation method was proposed by only measuring the primary input power. However, the estimation approach needs the exact value of the other parameters of the system. It is challenging to deal with the coupling variation since it cannot be measured directly. Recently, the control schemes considering the coupling variation have become a hot issue [13], [19], [20], [21], [22], [23], [24], [25]. A comparison of the mutual inductance estimation methods based on sensitivity analysis is made in [19], but all the techniques are offline, which is unsuitable for online control. Furthermore, an online inductance estimation has been proposed in [26]. Nevertheless, the estimation approach needs the exact value of the other parameters of the system.

The load voltage must be regulated when the IPT system charges the electric vehicle battery or directly feeds the electric vehicle motor drive. Therefore, methods to regulate the output voltage are discussed in the literature [27]. Adjusting the system operating frequency to regulate the output voltage reduces the efficiency [28], [29]. On the other hand, maintaining a constant output voltage by using a secondary inverter means more hardware [27]. Moreover, using an additional inverter on the primary side to regulate the output voltage has the same disadvantage [29].

This paper attempts to mitigate the problem by proposing a new model-free predictive control (MFPC) for IPT systems based on frequency optimization. Data from the latest state of the system is used in calculating the equivalent input reactance to predict the following state and find an optimum frequency. Also, an estimation has been presented to decrease the previous sample data. By applying the new proposed control system, the dependency on system parameters is eliminated. Moreover, the stagnation issue is avoided as the look-up table used in conventional methods is excluded in the proposed method. The optimal frequency is applied to the system using the proposed group-based method, while system-unsafe operating points are avoided. Moreover, a high computational burden is not imposed on the processor. The control scheme merely uses the information of inverter voltage and current obtained by two available onboard sensors. The simulation and experimental results confirm the effectiveness of the proposed method.

II. SYSTEM MODELING AND CIRCUIT ANALYSIS

The equivalent circuit of the system modeled as shown in Fig. 1. The primary and secondary windings are modeled with their inductances L_p and L_s, and their corresponding resistances r_1 and r_2. The capacitors C_p and C_s are also employed to compensate the system reactive power. The KVL equations of the circuit can be written as [30]:

$$U_{in} = z_1 i_1 - j\omega M i_2, \tag{1}$$

$$z_2 i_2 - j\omega M i_1 = 0, \tag{2}$$

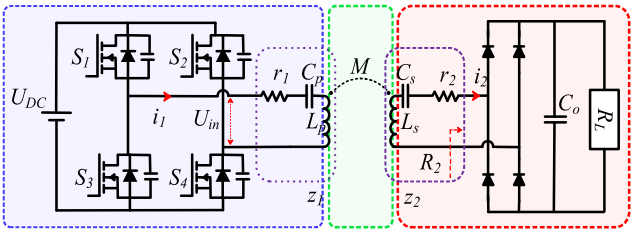

FIGURE 1. AN IPT system model with series-series compensation.

where, z_1, z_2, M, and ω represent the primary and secondary-side impedance of the system, the mutual inductance of the primary and secondary sides and the angular frequency of the inverter. z_1 and z_2 can be given as:

$$z_1 = r_1 + j\omega L_p + 1/j\omega C_p, \tag{3}$$

$$z_2 = r_2 + R_2 + j\omega L_s + 1/j\omega C_s. \tag{4}$$

where, R_2 refers to the equivalent ac load resistance seen from rectifier. It can be obtained as:

$$R_2 = \frac{8}{\pi^2} R_L. \tag{5}$$

Also, the input impedance of the system can be written as:

$$z_{in} = z_1 + M^2\omega^2 / z_2, \tag{6}$$

Litz wire is used in IPT windings in order to provide negligible ESR (r_1 and r_2). Moreover, small value of converter on-resistance can be dismissed if suitable MOSFETs are employed [31]. *PF* is a pivotal factor that can be considered as criterion of system competence. It can be express as:

$$PF = \cos\left(\tan^{-1}\left(\frac{X_i}{R_i}\right)\right), \tag{7}$$

where X_i and R_i are imaginary part and real part of impedance seen from output of the inverter, respectively. The imaginary part of z_{in} must be minimized in order to maximize the input *PF*. It can be expressed as follows:

$$X_i = L_p\omega - \frac{1}{C_p\omega} + \frac{M^2\omega(1 - L_sC_s\omega^2)}{R_2^2C_s + C_s\left(L_s\omega - (C_s\omega)^{-1}\right)^2}, \tag{8}$$

Also, the R_i can be written as follows:

$$R_i = \frac{M^2\omega^2R_2}{R_2^2 + \left(L_s\omega - (C_s\omega)^{-1}\right)^2}. \tag{9}$$

By using (7)- (9), PF can be plotted in different operating points.

It's of benefit to assume the following inequality:

$$R_2^2 \gg \left(L_s\omega - (C_s\omega)^{-1}\right)^2. \tag{10}$$

It can be acclaimed that the assumption mentioned in (10) is valid considering the parameters determined by the standard SAEJ2954. In the proposed standard for WPT2, the maximum of the load power is 7.7 kVA and the output voltage has a specified range (280V- 420V) [32]. As it can be seen in [32], the frequency range can be varied between 79- 90 kHz for the application the same as one in this paper. Higher frequencies in MHz ranges can be also used in IPT systems depending on the applications which EV charging is not included there. To Verify (10), the worst case is assessed. Considering minimum value of output voltage, $V_o = 280$ V, the equivalent output load resistance can be defined as $R_2 > 11\Omega$. In this paper, the IPT system is designed for class Z2. Accordingly, the inductance and compensator capacitance values are selected as $L_s = 44$uH, $C_s = 92$nF, and $f_{rs} = 79000$ Hz. In the worst case, the inverter's operating frequency and the secondary-side have the most considerable allowable difference, so it can be considered that $f_o = 90000$ Hz. So, (10) can yields $(L_s\omega\text{-}(C_s\omega)^{-1})^2 = 21.6$. On the other hand, as mentioned above, it is always $R_2^2 > 11^2\Omega\ R_2^2 > 11^2\Omega R_2^2 > 11^2\Omega$. As a result, the following inequality can be expressed and it can be argued that (10) is correct:

$$\frac{R_2^2}{\left(L_s\omega - (C_s\omega)^{-1}\right)^2} > 4. \tag{11}$$

By using (10) in (8), it yields:

$$X_i = \frac{-M^2L_s\omega^3}{R_2^2} + L_p\omega + \frac{M^2\omega}{C_sR_2^2} - \frac{1}{C_p\omega}. \tag{12}$$

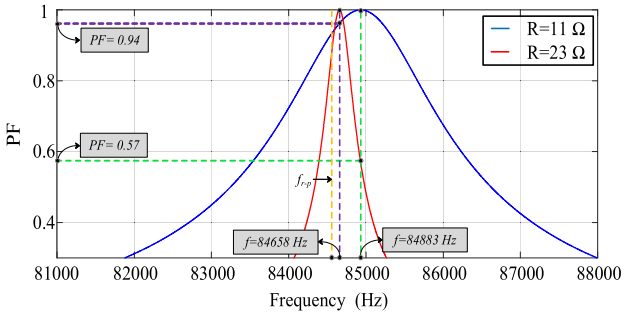

FIGURE 2. *PF* vs frequency in different loads resistances when $f_{r-p} \neq f_{r-s}$, and k = 0.1.

III. PF AND MFPC ANALYSIS

A. ANALYSIS OF SYSTEM POWER FACTOR

Finding an optimal operating frequency to maximize *PF*is sought in this section. This is performed by plotting input *PF*using (7)- (9) versus the operating frequency in Figs. 2 and 3, according to (1) and (4) and using the parameters given in TABLE 1. It is noteworthy that the operating frequency in the primary and secondary sides are the same. It has been studied in the literature in case of equal resonant frequencies of primary, f_{r-p}, and secondary, f_{r-s}, the input power factor will be unity [5]. Nevertheless, there is no assurance that f_{r-p} and f_{r-s} to be equal in practical cases. In fact, the onboard circuits of the dynamic charging systems are not the same for various EVs. On the other hand, even if they may be the same, it is possible that the circuit parameters change due to the aging of the components or misalignment of EVs.

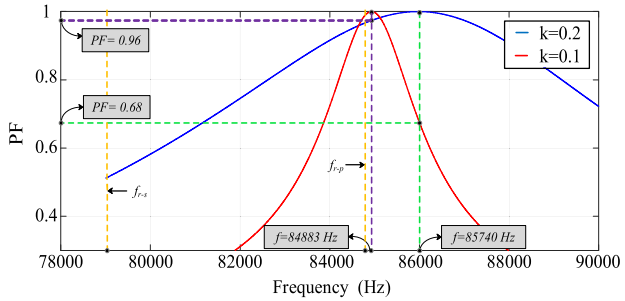

FIGURE 3. *PF* vs frequency in different coupling coefficients when $f_{r-p} \neq f_{r-s}$, and R = 11 Ω.

TABLE 1. Parameters of the system.

Parameter		Value
L_p	Primary -side Inductance	35 µH
L_s	Secondary-side Inductance	44 µH
C_p	Primary compensation capacitor	101 nF
C_s	Secondary compensation capacitor	92 nF
R_L	Load resistance	11 Ω
f_{rp}	Resonant frequency of primary side	85000 Hz
f_{rs}	Resonant frequency of secondary side	79000 Hz
U_{DC}	DC input voltage	40 V

In Fig. 2, *PF* of the system is plotted for $R = 11\ \Omega$ and 23 Ω loads. In case of unequal f_{r-p} and f_{r-s},the optimal operating frequency has a distinctively different values at different loads.Furthermore, as shown in Fig. 2, if the system load changes from 11 Ω to 23 Ω and the operating frequency remains constant, the input *PF* drops significantly. Hence, the system may enter unsafe operating points. It is noteworthy that a decrease in *PF* reduces the system power utilization rate. On the other hand, the effect of coupling coefficient variation on *PF* has been shown in Fig. 3. It can be seen, the optimum operating frequency to realize the unity power factor varies in different coupling coefficients. In addition, it can be obtained that the *PF* deviation in terms of the frequency changes by the load and coupling coefficient. Furthermore, *PF* decreases remarkably if the k changes and the operating frequency does not. Hence, it can be deduced that with unequal f_{r-p} and f_{r-s}, the realizing high *PF* is subject to tune the operating frequency. As it can be seen from Figs. 2 and 3, the optimum frequency, where the *PF* becomes highest value (with the parameters mentioned in TABLE 1 highest PF = 1) can be either between the primary and secondary resonance frequency or out of that depending on the system characteristics. So, it can be said the optimum operating frequency is not following the specific trend. Therefore, it is necessary to find the optimum operating frequency using a model-independent algorithm in order to provide unity power factor. So, the proposed control method should be robust, fast, and independent of previous operating point. Such algorithm has not been studied for IPT systems in the literature. In this paper, it is intended to maximize *PF* with the highest dynamics in IPT systems using a model-free predictive algorithm and considering unequal f_{r-p} and f_{r-s}.

B. MFPC IMPLEMENTATION ANALYSIS

According to (8), it can be stated that *PF*is a function of system parameters. As a first step to achieving a model-free control system, (8) can be rewritten as follows in order to get rid of the negative effect of parameter dependency.

$$X_i = \alpha\omega^3 + \beta\omega + \frac{\gamma}{\omega}, \tag{13}$$

The terms α, β, and γ can be expressed as functions of the system parameters, which are called mega parameters, as given as follows:

$$\alpha = \frac{-M^2 L_s}{R_2^2}, \tag{14}$$

$$\beta = L_p + \frac{M^2}{C_s R_2^2}, \tag{15}$$

$$\gamma = \frac{-1}{C_p}, \tag{16}$$

Discretized form of (13) can be expressed as follows:

$$X_i[m] = \alpha\omega^3[m] + \beta\omega[m] + \frac{\gamma}{\omega[m]}, \tag{17}$$

X_i in the [z]th sampling interval is defined as follows by using the normal forward Euler approximation.

$$X_i[m+z] = \alpha\omega^3[m+z] + \beta\omega[m+z] + \frac{\gamma}{\omega[m+z]}. \tag{18}$$

Also, it has been supposed that the system parameter divagation has a slow rate compared with the control sampling frequency, especially in the short time interval of sampling intervals. So, it is credible to consider that the *PF* varies only if the operating frequency changes. The left side of (13) is calculated using only the two sensors in the inverter output as follows:

$$X_i = \frac{V_{1,rms}}{i_{1,rms}} \sin\varphi_1, \tag{19}$$

where $V_{1,rms}$, $i_{1,rms}$, and φ_1 represent the rms of fundamental harmonic of inverter voltage, rms of fundamental harmonic of inverter current and the phase difference between the voltage and inverter current fundamental harmonics, respectively. By discretizing and using the normal forward Euler approximation, X_i in the [z]th sampling interval are defined as:

$$X_i[m+z] = \frac{V_{1,rms}[m+z]}{i_{1,rms}[m+z]} \sin\varphi[m+z]. \tag{20}$$

In this paper, unlike the conventional MFPC method, which has been implemented in other power electronics fields, the samples are discretized in the frequency domain instead of the time domain. The objective is to minimize the computational burden and overcome the equipment limitations. As seen in (18), $X_i[m+z]$ is expressed as a direct function of three parameters. Using the three last sampled data of the inverter, one can calculate α, β, and γ. In other words, it has been supposed that the system is operating in the optimum frequency which results in optimum *PF*. After an abrupt change in load

or coupling coefficient, two other frequencies are needed to calculate the new mega parameters of the system. To keep the safety margin and decrease the voltage and current stresses across the switches in practice, the minimum permissible frequency according to the SAEJ2954 is applied to the system. The other frequency which should be applied to the system is the average of two recent applied frequencies. Notably, if the intelligent assumption (10) has not been implemented, more than six previous data were required. Finally, the terms can be used to predict the next value of X_i in the next sampling interval as follows.

$$X_i[m-1] = \alpha\omega^3[m-1] + \beta\omega[m-1] + \frac{\gamma}{\omega[m-1]}. \quad (21)$$

IV. CV CHARGING MODE ANALYSIS

Using (1) and (2), the voltage across the load voltage can be express as (22):

$$V_{load} = \frac{U_{DC} M \omega_o R_2 Sin(D_i)}{\sqrt{\left(\frac{R_2}{C_p\omega_o}\left(\frac{\omega_o^2}{\omega_p^2}-1\right)+M^2\omega_o^2\right)^2+\left(\frac{\left(\frac{R_2}{C_p\omega_o}\left(\frac{\omega_o^2}{\omega_p^2}-1\right)\right)^2}{M^2\omega_o^2}\right)^2}}, \quad (22)$$

where U_{DC} is the input voltage of the inverter. According to (21), the load voltage is a function of D_i and f_o.

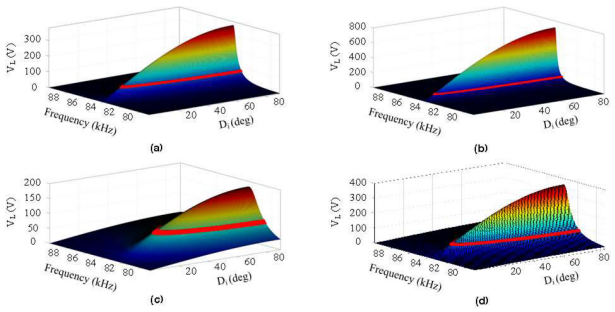

FIGURE 4. Load voltage vs frequency and inverter duty ratio in different loads and coupling coefficients; (a) $R_L = 11\Omega$ and $k = 0.1$, (b) $R_L = 22\Omega$ and $k = 0.1$, (c) $R_L = 11\Omega$ and $k = 0.2$, (d) $R_L = 22\Omega$ and $k = 0.2$.

Four plots of load voltage versus operating frequency and duty cycle of inverter under different values of $k$and $R2$has been depicted in Fig. 4. The reference value of the load voltage has been specified on 80V with a red line in Fig. 4. As can be seen the reference voltage is provided by multiple pairs of f_o and D_i. However, due to power factor optimization, only one of the sets of operating points is selected as the optimal pair of operating point. As a result, it can be said that the system has a unique set of operating point.

The maximum load voltage is obtained by assuming $D_i = 1$ in (22). The maximum possible load voltage, $V_{L,max}$, is depicted versus the operating frequency in Fig. 5, using the parameters given in TABLE 1. According to Fig. 5, for weak

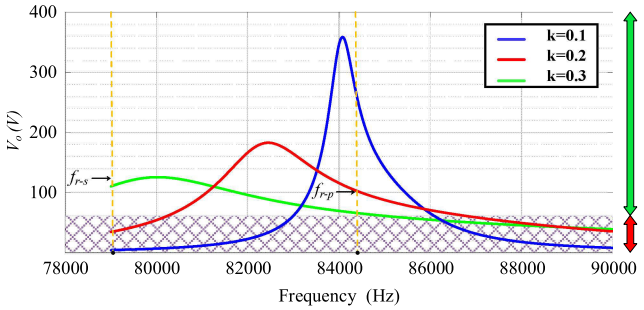

FIGURE 5. Maximum load voltage versus frequency.

coupling coefficients, the peak value increases due to the more substantial effect of M in the denominator of (20) compared with its nominator. Moreover, it is seen that the 80V load voltage cannot be provided for some operating frequencies even with $D_i = 1$.

Duty cycle of inverter is used to realize the CV charging mode. It can be concluded from (22) that any variation in coupling coefficient or load resistance should be pursued by D_i change in the CV charging mode. Hence, the controller can adjust D_i to keep the load voltage constant on its reference value. It can be concluded that, the proper value of D_i can be stated as:

$$D_i = \sin^{-1}\left(\frac{V_{ref}\sqrt{\left(\frac{R_2^2}{C_p^2M^2\omega_o^4}\left(\frac{\omega_o^2}{\omega_p^2}-1\right)+M^2\omega_o^2\right)^2+\left(\frac{R_2}{C_p\omega_o}\left(\frac{\omega_o^2}{\omega_p^2}-1\right)\right)^2}}{U_{DC}M\omega_o R_2}\right) \quad (23)$$

As seen in (23), operating frequency also performs its role in calculating the D_i. In order to prevent interference in adjusting the inverter duty ratio and operating frequency, the frequency tuning is set prior to the duty ratio adjustment. As a result, both control methods can achieve their goals simultaneously.

With the negligible losses as mentioned in section II, the reflected equivalent resistance in the primary side, R_e, can be written as follows:

$$R_e(\omega) = \frac{M^2\omega^2 R_2}{L_s^2\omega^2 + R_2^2 - \frac{2L_s}{C_s} + \frac{1}{C_s^2\omega^2}}, \quad (24)$$

Also, (24) can be rewritten as:

$$\frac{1}{R_e(\omega)} = \frac{L_s^2}{M^2R_2} + \frac{R_2^2C_s - 2L_s}{M^2R_2C_s\omega^2} + \frac{1}{M^2C_s^2R_2\omega^4}, \quad (25)$$

As it mentioned in (13), (24) can be express as:

$$\frac{1}{R_e(\omega)} = \delta + \frac{\sigma}{\omega^2} + \frac{\lambda}{\omega^4}, \quad (26)$$

where δ, σ,and λ can be written as:

$$\delta = \frac{L_s^2}{M^2 R_2}, \tag{27}$$

$$\sigma = \frac{R_2^2 C_s - 2L_s}{M^2 R_2 C_s}, \tag{28}$$

$$\lambda = \frac{1}{M^2 C_s^2 R_2}, \tag{29}$$

Using the three last sampled data of the inverter sensors, one can calculate δ, σ, and λ. In (22), R_2, M, and ω_p can be estimated using (13)- (15) and (26)- (28).

V. PROPOSED CONTROL METHOD

The proposed control scheme is intended to perform CV mode while making the system operate at the highest possible *PF*, even under abrupt load and k variations. They are elaborated on in this section.

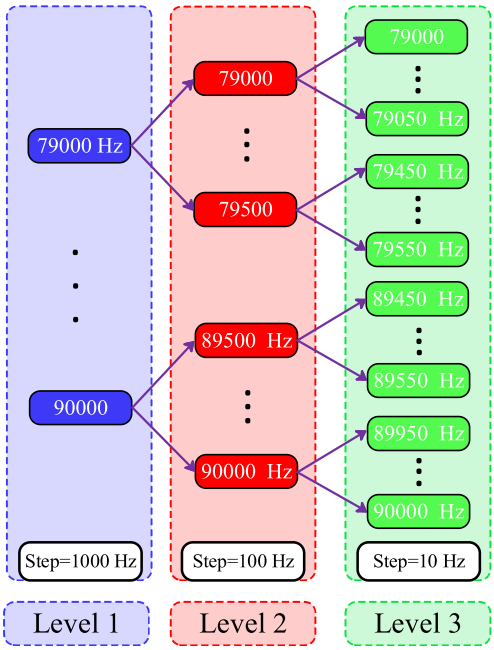

FIGURE 6. Schematic of the group-based control of frequency.

A. FREQUENCY OPTIMIZATION

Here, a group-based predictive method is used to find the optimal operating frequency. A view of the frequency groups has been depicted in Fig. 6. As can be seen the resolution of frequency increases in each level in compare of the previous level. The priority of frequency is round robin, and it can be said that no frequency has an inherently higher priority than others. In order to reduce the computation burden, increase the system dynamics, and avoid unsafe operating points, the full standard frequency range is divided into several level. The frequency range is categorized in the first level with an accuracy of 1000 Hz. Then, future values of the estimated inductance corresponding to each of the frequency variables are calculated using the cost function. The cost function is defined as follows:

$$CF^n = \left| X_i^{ref} - X_i^n[m-1] \right|. \tag{30}$$

where, superscript "n" and "ref" denote the number of group and reference values, respectively. Besides, $m$is the number of sampling instance.At the end of the first evaluation level, the optimum operating frequency is chosen from one of the first-level frequencies and is applied to the system. However, there is no guarantee that it would be the global optimum in the whole interval. In the second level of frequency tuning, the group that belongs to the applied frequency should be evaluated. It can be said the frequency step in the second level is reduced compared to the first level. Hence, the frequency chosen at this stage has higher accuracy than the previous one. The frequency tuning process continues until the *PF* reaches its reference value. It is noteworthy that in each tuning level, only one frequency is applied to the system. Thus, the imposition of transient current and voltage stresses is avoided.

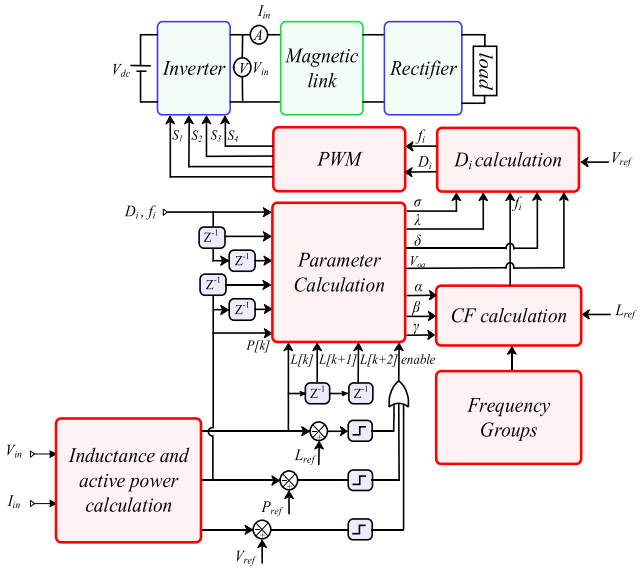

FIGURE 7. Schematic of the proposed control algorithm.

A block diagram of the proposed control system is shown in Fig. 7. Unlike the conventional model-free methods [17], this method does not require a look-up table, so there is no problem of stagnation. The proposed method uses only three inverters recent voltage, current, *PF*, and the corresponding frequency data to calculate the α, β, and γ to optimize the efficiency. Hence, the inductance estimation in the next step is free from the system parameters expressed in (20). The analysis is then used in (29) to calculate the cost function at each level of frequency tuning.

B. LOAD VOLTAGE REGULATION

Several methods have been proposed for voltage regulation usually by a particular converter [20]. The proposed method in this paper needs no converter for power or voltage

regulation as shown in Fig. 7. It is seen that the method estimates the system parameters, using (14)- (16) and (27)- (29). Then the controller adjusts D_i to perform the CV charging

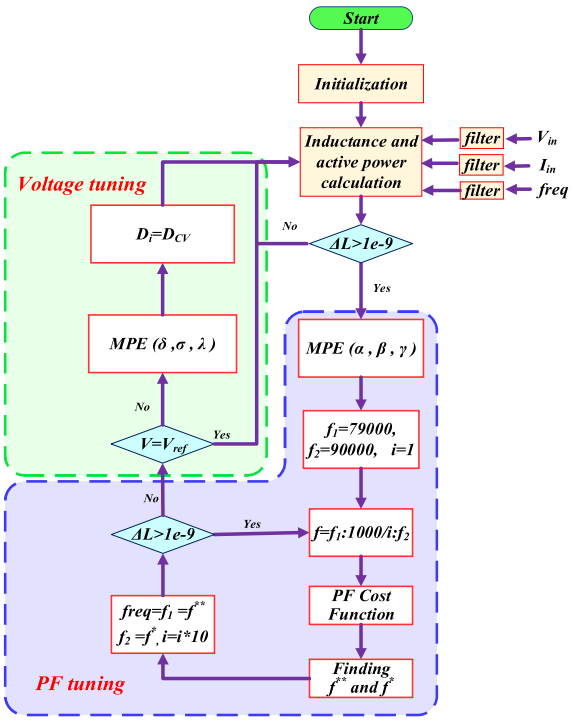

FIGURE 8. Flowchart of the proposed control algorithm.

Fig. 8 shows the flowchart of the model-free predictive control algorithm. In this method, only voltage and current sensors have been used on the primary side. In this method, the maximum value and the phase difference of the current and voltage signals of the inverter are measured. For this purpose, a simple saturator and peak detector circuit is used for the inverter current. It should be noted that the inverter output peak voltage is measured by a simple dc sensor on the DC-link. The calculation of voltage zero crossing is simple enough because D_i is provided by the processor directly. To prevent the sampling distortion, the filters calculate the average value of the last ten received data whenever new data is obtained as follows:

$$mean_{new} = 0.001(1000mean_{old} + data_{new} - mean_{old}). \tag{31}$$

In the case of a misalignment of the primary and secondary windings or load variation, the obtained PF decreases substantially. Therefore, the algorithm starts to find a new optimum frequency and duty cycle.

VI. PERFORMANCE EVALUATION

To evaluate the performance and validate the analytical results, the proposed mode-free predictive control scheme is evaluated through simulation and experimental result using MATLAB Simulink and a laboratory IPT system.

TABLE 2. Description of simulation setup.

Simulation	Simulation software	MATLAB/ SIMULINK
	Switches	IGBT with body diode
	Dynamic model implementation	Discrete inductance
	Magnetic link modeling	T model
	Simulation steps	2.5e-8

Moreover, a full description of the simulation setup is presented in TABLE 2.

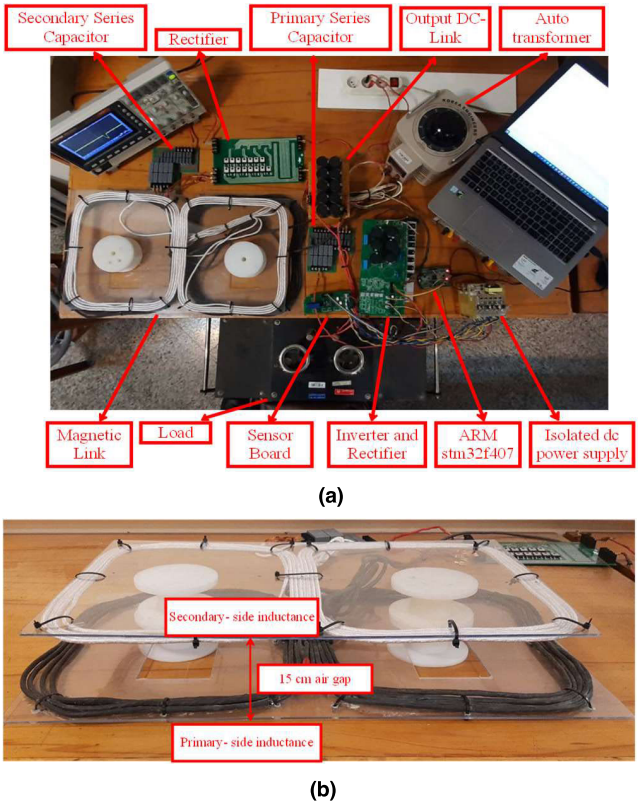

FIGURE 9. Experimental setup of the proposed IPT system; (a) general view, (b) magnetic link view.

A. SYSTEM IMPLEMENTATION

Fig. 9 shows the prototype setup of the proposed IPT system with a magnetic coupling link. The system includes a two DD type for primary and secondary side coils. According to class Z2, the air gap between the primary and secondary coils is set 10 cm in this system for $k = 0.2$. The primary side is supplied by a voltage source H-bridge inverter that provides a 3-level high- frequency voltage.

B. SIMULATION AND EXPERIMENTAL RESULTS

To evaluate the model-free predictive control performance and validate the analytical results, the proposed control scheme is evaluated through simulation and experimental results as depicted in Figs. 10-12 under the variations of

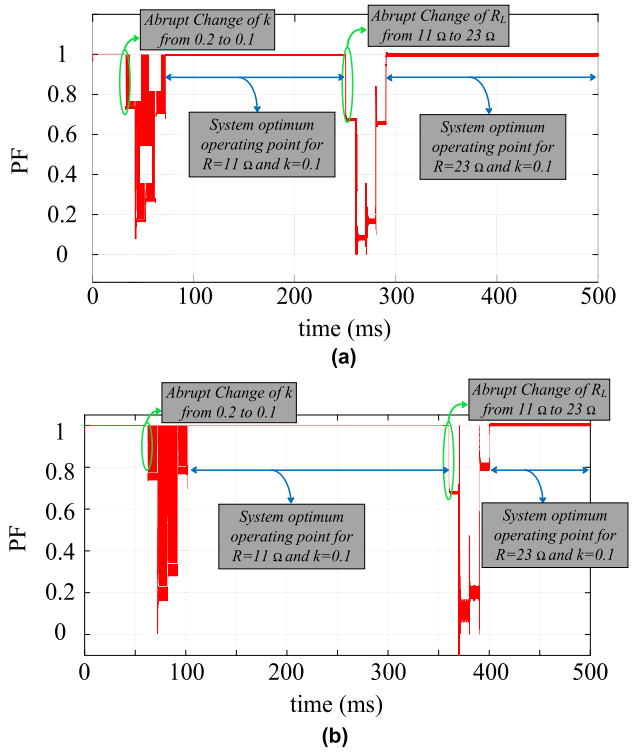

FIGURE 10. Input *PF* maximization considering change in the coupling coefficient and load resistance; (a) Simulation result, (b) Experimental result.

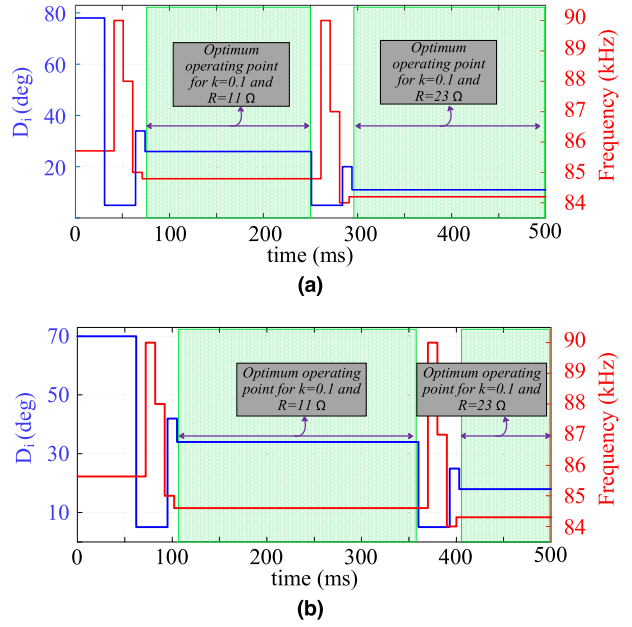

FIGURE 11. Tuning operating frequency and inverter duty ratio considering change in the coupling coefficient and load resistance; (a) Simulation result, (b) Experimental result.

coupling coefficient and load. The coupling change is modelled by abruptly changing air gap and relocating the pads manually. Also, the changes in output power are modeled in

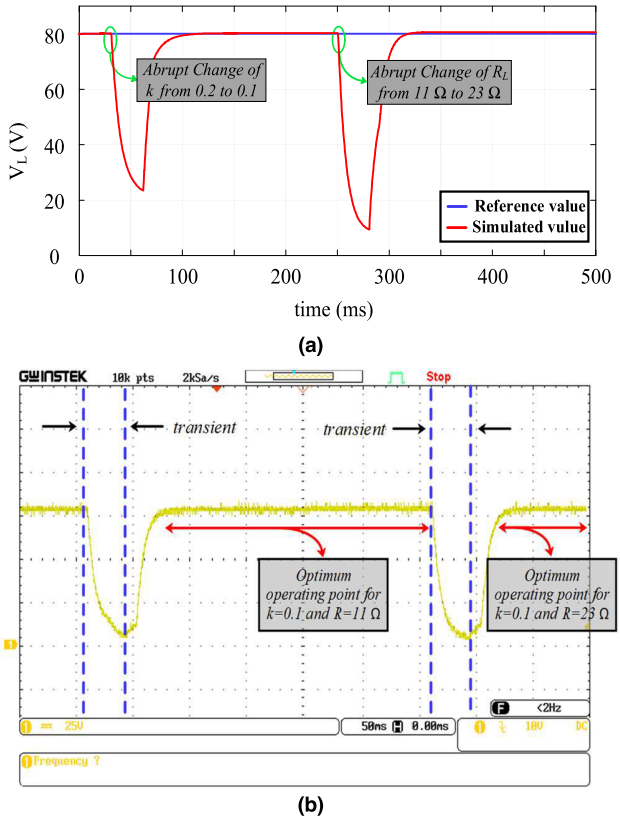

FIGURE 12. Load Voltage tuning considering change in the coupling coefficient and load resistance; (a) Simulation result, (b) Experimental result.

the setup by fast changes of output resistors. All practical data of frequency, duty cycle of inverter, and *PF* are extracted from the STM Studio software with the rate of *1Sample/ms*. The system parameters are presented in Table 1 and the reference voltage is set on $V_L = 80$V.

As stated in section II, the optimum frequency of the system is expected to change as the load resistance or k variation. A plot of *PF*for the IPT system, under the MFPC algorithm is depicted in Figs. 10 (a) and (b) by simulation and experimental results, respectively. As can be seen, after changing the k or R_L, the *PF* drops, and the process of finding the optimal frequency starts. In case of sudden coupling coefficient change at $t = 31$ ms and $t = 62$ ms in simulation and experimental results, respectively, *PF* reaches the optimal value in about 40 ms, in $t = 71$ ms and $t = 101$ ms s, by the simulation and experiment, respectively. Similarly, in case of load variation in $t = 251$ ms and $t = 360$ ms from 11Ω to 23Ω the *PF* is dropped again ms in simulation and experimental results, respectively. By tuning the frequency corresponding to the new load, *PF* is optimized at about 40ms at $t = 291$ ms and $t = 403$ ms in both simulations and experimental results, respectively. It can be seen that the system enjoys almost the same behavior in simulation and experiment.

Fig. 11 (a) and (b) compare the tuning process for the operating frequency as it finds its optimal value corresponding to

the maximum PF. It can be seen in Fig. 11 (a) and (b) that as soon as a sudden change in coupling coefficient or load, after three stages of applying the test frequency, the optimization process is performed in both simulations and experimental results. By changing the coupling coefficient, the optimal frequency is set at 84.8 kHz and 84.6 kHz in the simulation and experimental results, respectively, within 400 ms. After a sudden load change from 11Ω to 23Ω, the optimal frequency in the simulation and practical results reach 84.2 kHz and 84.3 kHz, respectively. The slight difference between the optimum frequency in simulation and implementation is due to neglecting losses of power converters and parasitic resistances. Moreover, D_i is still adjusted according to the new frequency to set the voltage at the reference value. As shown in Fig. 11, D_i is reduced to its minimum value when applying test frequencies to avoid violating system voltage and current limitations. After the end of the frequency test period, D_i is calculated and applied to the system. In next processing stage, the system operates at the optimal frequency, and D_i is applied to set the load voltage in the reference value. Hence, it can be claimed there is a good agreement between the simulation and experimental results for frequency and duty cycle optimization. As can be seen in Fig. 11, the number of frequencies applied to the system has decreased compared to the method mentioned in the literature [5]. On the other hand, the frequency is applied to the system intelligently, and the inverter is prevented to entering unsafe operating points. In addition, to prevent interference in adjusting the inverter duty ratio and operating frequency, the frequency tuning is set prior to the duty ratio adjustment. Moreover, the control process of the IPT system was performed without any information of the system, without data communication link between primary and secondary- sides and using only two available current and voltage sensors on the inverter.

The load voltage of the system is depicted in Fig. 12 (a) and (b) in the simulation and experimental results, respectively. It is seen in the case of a misalignment of the primary and secondary windings or load variations; the load voltage is regulated to its command value. As can be seen, during the test period, the load voltage is reduced to prevent damage. After the test period, which lasts about 30 ms, the new D_i corresponding to the frequency of the first layer is applied to the system. By applying the frequency corresponding to the second layer, D_i changes, and the load voltage is tuned at the 80V reference value.

The results of the proposed MFPC method is compared with the conventional methods(like PI controller), optimum tracking methods(P&O controller), and common predictive controller, which has been presented in TABLE 3. As it is shown, the optimum operating point of the DWPT system varies as the system characteristics change. Accordingly, model-based method (MPC) is not suitable for dynamic wireless charging though it achieves better dynamic response comparing to PI and P&O controllers. In contrast, the proposed MFPC method has fine accuracy against system parameter changes as well as an accepted dynamic response time.

TABLE 3. Comparison of common existing and proposed MFPC method.

Control type	Dynamic response	accuracy	Data calculation	feedback	Model dependency
MFPC	30 ms	Fine	Low	NO	NO
MPC [33]	~4 ms	*	Very high	YES	YES
PI Controller [1]	~350 ms	Fine	Low	YES	NO
P&O [5]	~1.5 s	Fine	Low	YES	NO

*: low accuracy in dynamic application where the model is not updated after an abrupt change in the system.

VII. CONCLUSION

An optimum frequency control for dynamic inductive power transfer systems has been proposed in this paper. The input PF dependency on circuit parameters in the case of unequal primary and secondary resonant frequency has been studied. A model- free predictive control method is presented to unravel the problem of parameter variation. The method uses only two already available on-board sensors of inverter voltage and current. The method works based on predicting the next value of inductance without using any parameters of the model. The next inductance value is used in the cost function to apply the optimal operating frequency in each level. The method prevents inverter to enter unsafe operating points. In order to reduce the computational burden, improve the system dynamics, and avoid unsafe operating points, the standard operating frequency range is divided into several groups that are selected in each optimization level. At each level, the frequency resolution increases ten times. In other words, using the proposed MFPC method the transient time will be reduced to 30 ms comparing to the literature which state long response time up to 400 ms. Furthermore, the communication link between the primary and secondary- sides has been removed, and the system can only be controlled by the frequency and duty ratio of the primary inverter. In order to prevent violating system, D_i is reduced to its minimum value when applying test frequencies. After the end of the frequency test period, D_i is calculated and applied to the system. Simulation results validate the effectiveness of the proposed system.

REFERENCES

[1] A. Babaki, S. Vaez-Zadeh, A. Zakerian, and G. A. Covic, "Variable-frequency retuned WPT system for power transfer and efficiency improvement in dynamic EV charging with fixed voltage characteristic," *IEEE Trans. Energy Convers.*, vol. 36, no. 3, pp. 2141–2151, Sep. 2021.

[2] A. A. S. Mohamed, A. Berzoy, and O. Mohammed, "Predictive active power-flow control of two-way wireless power transfer system in V2G services," in *Proc. IEEE 2nd Annu. Southern Power Electron. Conf. (SPEC)*, Dec. 2016, pp. 1–6.

[3] S. Hasanzadeh, S. Vaez-Zadeh, and A. H. Isfahani, "Optimization of a contactless power transfer system for electric vehicles," *IEEE Trans. Veh. Technol.*, vol. 61, no. 8, pp. 3566–3573, Oct. 2012.

[4] B. X. Nguyen, D. M. Vilathgamuwa, G. H. B. Foo, P. Wang, A. Ong, U. K. Madawala, and T. D. Nguyen, "An efficiency optimization scheme for bidirectional inductive power transfer systems," *IEEE Trans. Power Electron.*, vol. 30, no. 11, pp. 6310–6319, Nov. 2015.

[5] A. Zakerian, S. Vaez-Zadeh, and A. Babaki, "A dynamic WPT system with high efficiency and high power factor for electric vehicles," *IEEE Trans. Power Electron.*, vol. 35, no. 7, pp. 6732–6740, Jul. 2020.
[6] J. Liu, K. W. Chan, C. Y. Chung, N. H. L. Chan, M. Liu, and W. Xu, "Single-stage wireless-power-transfer resonant converter with boost bridgeless power-factor-correction rectifier," *IEEE Trans. Ind. Electron.*, vol. 65, no. 3, pp. 2145–2155, Mar. 2018.
[7] W. K. Mo, K. Paasch, and T. Ebel, "A complete optimal air gapped PFC boost inductor design for power converter applications," in *Proc. IEEE 13th Int. Symp. Power Electron. Distrib. Gener. Syst. (PEDG)*, Jun. 2022, pp. 1–6.
[8] J. T. Boys, C.-Y. Huang, and G. A. Covic, "Single-phase unity power-factor inductive power transfer system," in *Proc. IEEE Power Electron. Spec. Conf.*, Jun. 2008, pp. 3701–3706.
[9] S. Nvaiyan-Kalat, S. Vaez-Zadeh, and A. Zakerian, "Maximum power per current control for dynamic WPT systems," in *Proc. 12th Power Electron., Drive Syst., Technol. Conf. (PEDSTC)*, Feb. 2021, pp. 1–5.
[10] D.-H. Kim, M.-S. Kim, and H.-J. Kim, "Frequency-tracking algorithm based on SOGI-FLL for wireless power transfer system to operate ZPA region," *Electronics*, vol. 9, no. 8, p. 1303, 2020.
[11] M. J. Neath, A. K. Swain, U. K. Madawala, and D. J. Thrimawithana, "An optimal PID controller for a bidirectional inductive power transfer system using multiobjective genetic algorithm," *IEEE Trans. Power Electron.*, vol. 29, no. 3, pp. 1523–1531, Mar. 2014.
[12] Y. Yang, W. Zhong, S. Kiratipongvoot, S.-C. Tan, and S. Y. R. Hui, "Dynamic improvement of series–series compensated wireless power transfer systems using discrete sliding mode control," *IEEE Trans. Power Electron.*, vol. 33, no. 7, pp. 6351–6360, Jul. 2018.
[13] S. Kouro, "Model predictive control—A simple and powerful method to control power converters," *IEEE Transactions Ind. Electron.*, vol. 56, no. 6, pp. 1826–1838, Jun. 2008.
[14] S. Navaiyan-Kalat, S. Vaez-Zadeh, A. Babaki, and M. Pakzaban, "Model predictive control of a single stage power factor correction for inductive power transfer systems," in *Proc. 14th Power Electron., Drive Syst., Technol. Conf. (PEDSTC)*, Jan. 2023, pp. 1–6.
[15] M. Khalilzadeh, S. Vaez-Zadeh, J. Rodriguez, and R. Heydari, "Model-free predictive control of motor drives and power converters: A review," *IEEE Access*, vol. 9, pp. 105733–105747, 2021.
[16] L. Chen, S. Shao, Q. Xiao, L. Tarisciotti, P. W. Wheeler, and T. Dragicevic, "Model predictive control for dual-active-bridge converters supplying pulsed power loads in naval DC micro-grids," *IEEE Trans. Power Electron.*, vol. 35, no. 2, pp. 1957–1966, Feb. 2020.
[17] L. Chen, L. Lin, S. Shao, F. Gao, Z. Wang, P. W. Wheeler, and T. Dragicevic, "Moving discretized control set model-predictive control for dual-active bridge with the triple-phase shift," *IEEE Trans. Power Electron.*, vol. 35, no. 8, pp. 8624–8637, Aug. 2020.
[18] K. Song, Z. Li, J. Jiang, and C. Zhu, "Constant current/voltage charging operation for series–series and series–parallel compensated wireless power transfer systems employing primary-side controller," *IEEE Trans. Power Electron.*, vol. 33, no. 9, pp. 8065–8080, Sep. 2018.
[19] F. Liu, "A selection method of mutual inductance identification models based on sensitivity analysis for wireless electric vehicles charging," in *Proc. IEEE Energy Convers. Congr. Expo. (ECCE)*, Sep. 2016, pp. 1–6.
[20] Y. G. Su, H. Y. Zhang, Z. H. Wang, A. P. Hu, L. Chen, and Y. Sun, "Steady-state load identification method of inductive power transfer system based on switching capacitors," *IEEE Trans. Power Electron.*, vol. 30, no. 11, pp. 6349–6355, Nov. 2015.
[21] J. Yin, D. Lin, T. Parisini, and S. Y. Hui, "Front-end monitoring of the mutual inductance and load resistance in a Series–Series compensated wireless power transfer system," *IEEE Trans. Power Electron.*, vol. 31, no. 10, pp. 7339–7352, Oct. 2016.
[22] X. Dai, X. Li, Y. Li, and A. P. Hu, "Maximum efficiency tracking for wireless power transfer systems with dynamic coupling coefficient estimation," *IEEE Trans. Power Electron.*, vol. 33, no. 6, pp. 5005–5015, Jun. 2018.
[23] R. Mai, B. Yang, Y. Chen, N. Yang, Z. He, and S. Gao, "A misalignment tolerant IPT system with intermediate coils for constant-current output," *IEEE Trans. Power Electron.*, vol. 34, no. 8, pp. 7151–7155, Aug. 2019.
[24] F. Liu, K. Chen, Z. Zhao, K. Li, and L. Yuan, "Transmitter-side control of both the CC and CV modes for the wireless EV charging system with the weak communication," *IEEE J. Emerg. Sel. Topics Power Electron.*, vol. 6, no. 2, pp. 955–965, Jun. 2018.
[25] A. Zakerian, S. Vaez-Zadeh, A. Babaki, and M. F. Moghaddam, "Efficiency optimization of a dynamic wireless EV charging system using coupling coefficient estimation," in *Proc. 10th Int. Power Electron., Drive Syst. Technol. Conf. (PEDSTC)*, Feb. 2019, pp. 629–634.
[26] B. K. Bose, "Neural network applications in power electronics and motor drives—An introduction and perspective," *IEEE Trans. Ind. Electron.*, vol. 54, no. 1, pp. 14–33, Feb. 2007.
[27] H. Li, J. Li, K. Wang, W. Chen, and X. Yang, "A maximum efficiency point tracking control scheme for wireless power transfer systems using magnetic resonant coupling," *IEEE Trans. Power Electron.*, vol. 30, no. 7, pp. 3998–4008, Jul. 2015.
[28] N. Y. Kim, K. Y. Kim, J. Choi, and C.-W. Kim, "Adaptive frequency with power-level tracking system for efficient magnetic resonance wireless power transfer," *Electron. Lett.*, vol. 48, no. 8, pp. 452–454, Apr. 2012.
[29] C.-S. Wang, O. H. Stielau, and G. A. Covic, "Design considerations for a contactless electric vehicle battery charger," *IEEE Trans. Ind. Electron.*, vol. 52, no. 5, pp. 1308–1314, Oct. 2005.
[30] D. H. Tran, V. B. Vu, and W. Choi, "Design of a high-efficiency wireless power transfer system with intermediate coils for the on-board chargers of electric vehicles," *IEEE Trans. Power Electron.*, vol. 33, no. 1, pp. 175–187, Jan. 2018.
[31] J. Liu, G. Wang, G. Xu, J. Peng, and H. Jiang, "A parameter identification approach with primary-side measurement for DC–DC wireless-power-transfer converters with different resonant tank topologies," *IEEE Trans. Transport. Electrific.*, vol. 7, no. 3, pp. 1219–1235, Sep. 2021.
[32] J. Schneider, *Wireless Power Transfer for Light-Duty Plug-In/Electric Vehicles and Alignment Methodology*, document SAE International J2954 Taskforce, 2016.
[33] J. M. González-González, A. Triviño-Cabrera, and J. A. Aguado, "Model predictive control to maximize the efficiency in EV wireless chargers," *IEEE Trans. Ind. Electron.*, vol. 69, no. 2, pp. 1244–1253, Feb. 2022.

SINA NAVAIYAN KALAT was born in Tehran, Iran, in 1996. He received the B.Sc. degree in power systems engineering from the Department of Electrical Engineering, Ferdowsi University of Mashhad, Mashhad, Iran, in 2019, and the M.Sc. degree from the School of Electrical and Computer Engineering, University of Tehran, Iran, in 2023. His research interests include power electronics, wireless power transfer, AC–DC micro-grids, and renewable energies.

SADEGH VAEZ-ZADEH (Senior Member, IEEE) received the B.Sc. degree in electrical engineering from the Iran University of Science and Technology, Tehran, Iran, in 1985, and the M.Sc. and Ph.D. degrees in electrical engineering from Queen's University, Kingston, ON, Canada, in 1993 and 1997, respectively. In 1997, he joined the University of Tehran, Tehran, as an Assistant Professor and became an Associate Professor, in 2001, and a Full Professor, in 2005. Prior to this, he was with several research and educational institutions in different positions. He was the Head of the Power Department, University of Tehran, where he is currently the Director of the Advanced Motion Systems Research Laboratory, which he founded, in 1998. He has coauthored more than 200 research papers. He holds a U.S. patent. He is the author of the book *Control of Permanent Magnet Synchronous Motors*, (Oxford University Press, 2018); with its Chinese translation published, in 2022. His research interests include advanced rotary and linear electric machines and drives, wireless power transfer, renewable energy integration, and energy policy. He is a member of the Energy Internet Coordinating Committee, Motor Subcommittee, and the Power System Stability Control Subcommittee of the IEEE Power and Energy Society. He received several domestic and international awards for his contributions to the fields. He is an Editor of IEEE TRANSACTIONS ON SUSTAINABLE ENERGY and IEEE TRANSACTIONS ON ENERGY CONVERSION. He is a Subject Editor of *IET Renewable Power Generation*. He has been active in IEEE-sponsored conferences, as the General Chair, a keynote speaker, and a member of technical and steering committees.

ALI ZAKERIAN received the B.Sc. degree in electrical engineering from the K. N. Toosi University of Technology, Tehran, Iran, in 2016, and the M.Sc. degree in power engineering from the University of Tehran, Iran, in 2019. He is currently a Doctoral Researcher with Tampere University. Since 2016, he has been investigating wireless power transfer systems. His research interests include power electronics, wireless power transfer, and resonant converters.

AMIR BABAKI (Member, IEEE) received the B.Sc. and M.Sc. degrees in electrical engineering from the University of Tehran, Tehran, Iran, in 2012 and 2014, respectively, and the Ph.D. degree in power electronic from the School of Electrical and Computer Engineering, University of Tehran, in 2020. During his Ph.D., he has been active as a Visiting Researcher with the IPT Group, University of Auckland, New Zealand. He is currently with the Center for Industrial Electronics (CIE), University of Southern Denmark, Denmark, as a Postdoctoral Researcher. His research interests include inductive power transfer, active front end compact converter design, and electric vehicles.

THOMAS EBEL (Senior Member, IEEE) received the Dipl.-Chem. degree (M.Sc. equivalent) in chemistry from Münster University, in 1992, and the Ph.D. degree (Dr.rer.nat.) from the Institute of Inorganic Chemistry, Münster University, in 1995. In 1995, he has spent three months, as a Guest Researcher with CNRS, Institute des Matériaux de Nantes, France, with Prof. J. Rouxel. From August 1995 to September 2001, he was a Research and Development Engineer, and later the Research and Development Director of Siemens Matsushita Components, Siemens AG PR. Since October 1999, he has been with EPCOS AG; and since October 2008, he has been with TDK, Business Unit of Aluminum Electrolytic Capacitors, Heidenheim, Germany. From October 2001 to July 2008, he was the Research and Development Director, later the Technical Director (a CTO), and a member of the Board of Directors of Becromal Norway (Becromal S.p.A., since October 2008, Epcos, now TDK Foil), Milano, Italy. From September 2008 to July 2018, he was the Managing Director and a Shareholder with FTCAP GmbH (Husum Manufacturer of Aluminum Electrolytic and Film Capacitors), Germany. Since August 2018, he has been the Head of the Section of Electrical Engineering and the Centre for Industrial Electronics (CIE), University of Southern Denmark (SDU), Odense, Sønderborg. Since January 2022, he has been a Full Professor.